

Star Clusters in the Nearby Late-Type Galaxy NGC 1311¹

Paul B. Eskridge²

paul.eskridge@mnsu.edu

Richard de Grijs^{3,4}, Peter Anders⁵, Rogier A. Windhorst⁶, Violet A. Mager^{7,8}, & Rolf A. Jansen⁶

ABSTRACT

Ultraviolet, optical and near infrared images of the nearby ($D \approx 5.5$ Mpc) SBm galaxy NGC 1311, obtained with the *Hubble Space Telescope*, reveal a small population of 13 candidate star clusters. We identify candidate star clusters based on a combination of their luminosity, extent and spectral energy distribution. The masses of the cluster candidates range from $\sim 10^3$ up to $\sim 10^5 M_{\odot}$, and show a strong positive trend of larger mass with increasing with cluster age. Such a trend follows from the fading and dissolution of old, low-mass clusters, and the lack of any young super star-clusters of the sort often formed in strong starbursts. The cluster age distribution is consistent with a bursting mode of cluster formation, with active episodes of age ~ 10 Myr, ~ 100 Myr and $\gtrsim 1$ Gyr. The ranges of age and mass we probe are consistent with those of the star clusters found in quiescent Local Group dwarf galaxies.

¹Based on observations with the NASA/ESA Hubble Space Telescope, obtained at the Space Telescope Science Institute, which is operated by the Association of Universities for Research in Astronomy, Inc. under NASA contract No. NAS5-26555.

²Department of Physics and Astronomy, Minnesota State University, Mankato, MN 56001

³Department of Physics and Astronomy, University of Sheffield, Sheffield S3 7RH, United Kingdom

⁴National Astronomical Observatories, Chinese Academy of Sciences, Beijing, P.R. China

⁵Sterrenkundig Instituut, Universiteit Utrecht, NL-3508 TA Utrecht, The Netherlands

⁶School of Earth & Space Exploration, Arizona State University, Tempe, AZ 85287

⁷Department of Physics and Astronomy, Arizona State University, Tempe, AZ 85287

⁸Observatories of the Carnegie Institution of Washington, Pasadena, CA 91101

Subject headings: galaxies: individual (NGC 1311) — galaxies: spiral — galaxies: star clusters — infrared: galaxies — ultraviolet: galaxies

1. Introduction

Star clusters are powerful tools for probing the star-formation history and chemical enrichment of galaxies (e.g., Hodge 1961; Whitmore et al. 1999; Dolphin & Kennicutt 2002b; de Grijs et al. 2005). In nearby systems, star clusters provide us with spatially resolved examples of simple stellar populations (SSPs). Observations of individual cluster stars are, therefore, crucial for understanding the effect of metallicity on stellar evolution (e.g., Gallart et al. 2003 and references therein). In more distant systems, star clusters provide us with examples of unresolved SSPs. Analysis of statistical samples of such clusters offers us a wealth of information on the history of star formation in their parent galaxies (e.g., de Grijs et al. 2005 and references therein). Understanding star and cluster formation in a range of environments is essential for understanding galaxy evolution because star cluster formation traces the strongest episodes of galactic star formation (e.g., de Grijs et al. 2003b).

There has been a great deal of work on star cluster populations and formation histories in nearby luminous spiral galaxies over the last decade (e.g., Whitmore et al. 1999; de Grijs et al. 2005; Dolphin & Kennicutt 2002b; Larsen 2004). By comparison, the star cluster formation history in nearby, low-luminosity galaxies has received relatively little attention (but see, e.g., Billett et al. 2002; Anders et al. 2004a; Seth et al. 2004; de Grijs & Anders 2006). Studies of nearby galaxies are important because we can resolve abundant small-scale detail in them. Moreover, the low metallicities of low-luminosity nearby galaxies offer us a close-up view of the star-formation process that may better resemble that in the high-redshift, early Universe.

Studies of detailed stellar formation histories are still restricted to fairly nearby galaxies, and are most powerful when they combine high angular resolution with broad wavelength coverage. The number of very nearby galaxies with such data available is still quite small. NGC 1311 is a very nearby ($D \approx 5.5$ Mpc), but little-studied late-type (SBm) galaxy. Tully et al. (2006) identify it as a member of the 14+14 Association, a loose group dominated by the luminous spiral NGC 1313. Table 1 summarizes the basic properties of the system. NGC 1311 was a target in several *Hubble Space Telescope* (HST) snapshot surveys (GO programs 9124 and 9824; Windhorst et al. 2002, Taylor et al. 2005, and §2 below). As a result, a set of broad-band images spanning a wide wavelength interval (0.3–1.6 μ m) at sub-arcsecond resolution now exists for this galaxy. As NGC 1311 is quite nearby, the bright star clusters and luminous individual stars are detected as discrete sources. We can thus

probe the spatially resolved star-formation history of NGC 1311 by studying the broad-band spectral energy distributions of the star clusters, the individual stars, and the unresolved light. This paper is concerned with the star clusters of NGC 1311. We shall address the individual stars and unresolved light in future publications.

In §2 we describe the HST observational data. We present the observed properties of the candidate star clusters in §3, and our analysis of these observations in §4. We summarize our conclusions, and discuss issues for further research in §5.

2. Observational Data

The data for this study are a set of UV, optical and NIR images obtained with the Wide-Field and Planetary Camera 2 (WFPC2) and the Near Infrared Camera and MultiObject Spectrograph (NICMOS) on board HST. We have WFPC2 images taken through the F300W, F606W and F814W filters, and a NICMOS image taken with the NIC3 camera through the F160W filter. Details of the observations are given in Table 2. The F300W and F814W WFPC2 images were obtained as part of the HST program GO-9124 “Mid-UV Snapshot Survey of Nearby Irregulars: Galaxy Structure and Evolution Benchmark” (R. Windhorst PI). For these images, the nuclei of the target galaxies were placed on the WF3 chip. Details of the observing and reduction procedures for these data are given in Windhorst et al. (2002). The F160W image was obtained as part of the HST program GO-9824 “NIC3 SNAPs of Nearby Galaxies Imaged in the mid-UV: The Remarkable Cool Stellar Population in Late-Type Galaxies” (R. Windhorst PI). Details of the observing and reduction procedures for these data are given in Taylor et al. (2005). The archival WFPC2 F606W image of NGC 1311 was obtained as part of the HST program GO-9162 “Local Galaxy Flows and the Local Mass Density” (R. Tully PI). The WFPC2 Wide-Field Camera (WFC) spatial sampling is $\approx 0''.10$ per pixel. Our search for candidate star clusters turned up no examples on the WFPC2 Planetary Camera CCD, so we do not use the PC data in this study. The NIC3 spatial sampling is $0''.20$ per pixel. We show images of the central $42'' \times 26''$ of NGC 1311 in the four observed bands in Figure 1.

3. Candidate Star Clusters

Candidate star clusters in external galaxies can be identified in several ways. Physically large clusters in sufficiently nearby galaxies are extended sources. Compact star clusters, or star clusters in more distant galaxies can be identified by their luminosity in the most extreme

cases. Such clusters can also be distinguished from bright stars by their spectral energy distribution (SED). Whitmore et al. (1999), Anders et al. (2004a, 2007) and Bastian et al. (2005) give more detailed discussions of how to distinguish star clusters from individual luminous stars. We make use of both luminosity and SED criteria to define our list of candidate star clusters in NGC 1311.

We used HSTPhot⁷ (Dolphin 2000) to extract stellar photometry from the WFPC2 images. For the NICMOS image, we used the version of DAOPHOT (Stetson 1987) embedded in the XVISTA image analysis package (Stover 1988). We then selected candidate clusters by searching the output photometry files for sources that are either extended compared to the point-spread function (PSF), or have colors that deviate from those of individual stars. We discuss the details of our analysis below.

3.1. Stellar Photometry

HSTPhot is designed to perform stellar photometry on WFPC2 images, including aperture corrections, charge-transfer efficiency corrections, and zero-point calibrations. The zero-points to the VEGAMAG system are thus updated from those of Holtzman et al. (1995). For the NICMOS image, we first applied the non-linearity correction determined by de Jong (2006). This refines the zero-point calibration from the 2004 June standard (Noll et al. 2004). We then extracted stellar photometry with XVISTA/DAOPHOT. For the NICMOS photometry, we had to determine the aperture correction manually by measuring the asymptotic count rates for two bright, isolated stars in the observed field. The correction from the 2-pixel radius to infinite aperture is 0.10 ± 0.02 magnitudes. All of our photometry is calibrated to the VEGAMAG system.

We compare our stellar photometry to isochrones derived from the models of Girardi et al. (2002). In order to plot the isochrones with the photometry, we need an estimate of the distance to NGC 1311. The best available distance estimate for NGC 1311 is that of Tully et al. (2006), who quote $D = 5.45$ Mpc based on the magnitude of the tip of the red giant branch. There appear to be no metallicity measurements of NGC 1311 in the literature. For the distance quoted above, we find that the isochrones with $Z = 0.004$ provide the best visual fit to the CMDs. The more metal-poor isochrones have upper main sequences that are substantially bluer than observed in all available colors. The isochrones more metal-rich than $Z = 0.008$ do not predict stars luminous enough in the ultraviolet compared to the data. We defer a

⁷We used the May 2003 revision of HSTPhot v. 1.1.5b obtained from http://purcell.as.arizona.edu/wfpc2_calib/.

more detailed discussion of the isochrone fitting to our paper on the stellar photometry. We adopt a metallicity of $Z = 0.004$ below unless otherwise noted.

3.2. Identification of Cluster Candidates

There are a number of objects that are not well-fit by the isochrones in color-color diagrams. Figure 2 shows two color-color diagrams that demonstrate the problem. There are objects that are bluer than the isochrones for short-wavelength filter combinations and redder than the isochrones for long-wavelength filter combinations. Several of the oddly colored objects are within 3σ of the photometric limits in at least one bandpass. In those cases, we adopt the conservative view that the odd colors are likely caused by relatively large errors near the photometric limit. We note that a large fraction of the points shown in Fig. 2 deviate from the isochrones. This is due to a selection bias. There are a relatively small number of normal stars that are bright enough at both 3000\AA and at 8000\AA to be detected in both F300W and F814W.

In Figure 3, we show an example of a stellar color–magnitude diagram (CMD) with the objects with secure measurements of their anomalous colors marked with large circles and those with uncertain measurements, too near the relevant photometric limits, enclosed within large diamonds. In practice, we impose a magnitude limit of $I_{814} < 22$ on objects selected by their photometric peculiarity. This is a simple cut-off to impose, and we found that objects fainter than this limit have color uncertainties large enough that their deviation from the isochrones in color-color plots are not statistically significant. A number of objects are substantially brighter than this faint limit, and still have colors that deviate from the isochrones by more than 2σ . On this basis, we consider them to be candidate star clusters. Figure 4 shows a portion of the F606W image with the photometrically selected candidate clusters circled. We note that the faintest cluster candidates so identified have apparent magnitudes of $V_{606} \approx 22.6$, or absolute magnitudes of $M_{606} \approx -6.1$.

A stellar cluster with an age of ~ 10 can have extremely red supergiants dominating the red and NIR bands, as well as hot blue main sequence stars dominating the blue and NUV bands. At ages of ~ 100 Myr, the red spectrum can be dominated by luminous asymptotic giant branch stars and the blue spectrum by blue supergiants (Persson et al. 1983; Maraston 2005). This will cause the integrated colors of such a cluster to appear blue in bands dominated by the luminous blue stars, and red in bands dominated by the luminous red stars; exactly the phenomenon demonstrated in Fig. 2, and one that has been well known to apply to Magellanic Cloud clusters for many years (Persson et al. 1983). We note that the candidate clusters do not stand out in the CMD (see Fig. 3). It is only in the

color-color diagrams that their peculiarity becomes evident. This is in keeping with the results of Bastian et al. (2005), who showed that broad wavelength sampling of the SED could discriminate between star clusters and luminous single stars.

The HSTPhot output includes a number of parameters that are useful in distinguishing extended sources from point sources. These are discussed in detail by Dolphin (2000). The χ parameter is a goodness-of-fit parameter derived from the standard statistical χ^2 . A good, well-fit stellar image in an uncrowded field should have $\chi \lesssim 1.5$. Sources with χ much greater than this are candidate star clusters, but can also include stellar blends and background galaxies. The sharpness parameter is zero for a perfectly-fit stellar image, negative for objects more extended than the PSF, and positive for artifacts that are too sharp (cosmic rays, for instance). A stellar PSF image in a relatively uncrowded field should have a sharpness of 0 ± 0.5 . A plot of the sharpness parameter, output from HSTPhot, against V_{606} is shown in Figure 5. The figure indicate that there are plausible cluster candidates up to a magnitude fainter than the candidates found above. Fainter than $V_{606} \approx 24$ mag, the HSTPhot-identified “extended sources” are consistent with the outer envelope of point sources in the V_{606} –sharpness plot. They are thus not significantly extended in our data. However, there is a group of nine sources with $22.4 \leq V_{606} \leq 23.6$ that are clearly offset from the stellar locus in this magnitude range (see Fig. 5). None of these sources have colors that distinguish them from the stellar isochrones at a statistically significant level. We indicate these extended sources by diamonds in Figure 6. Two of them are obvious background spirals, and two more are likely background objects. These four are labelled “bg” in Fig. 6, and shown by large, dark crosses in Fig. 5. The remaining five sources are additional faint candidate clusters in NGC 1311, bringing the total to 13. Postage stamp images from the F606W data, centered on the candidate clusters, and oriented as in Fig. 6, are shown in Figure 7. Each postage stamp measures $6''.5$ square.

We make no formal assessment of our completeness level, as this is not critical for our current purposes. However, we point out that we are unlikely to have missed any luminous clusters ($V_{606} \lesssim 22$), even in the most crowded part of the field. At fainter magnitudes, our census is certainly incomplete. Thus we make no attempt to quantify the cluster formation rate. We shall address the completeness function (for point sources) in our paper on the individual stars in NGC 1311.

4. Discussion

4.1. Extendedness Tests

We see from Fig. 7 that several of the cluster candidates are quite compact. For an object at a distance of 5.45 Mpc a WFC pixel subtends only about 2.6 pc. Thus unresolved sources are either very compact, or they are foreground/background point sources. The simplest way to test for extendedness is to plot the radial profiles of the candidate clusters along with those of stars. We show such plots in Figure 8. Cluster candidates 1, 5, 6, 10 and 12 are not significantly more extended than stars in their vicinity. The remaining sources are clearly extended at WFPC2 resolution. This is consistent with the HSTPhot results shown in Fig. 5.

Globular star clusters in the Milky Way have an average half-light radius of $R_{hl} \approx 3.3 \pm 1.7$ pc (determined from the database of Harris 1996⁸, not including the distant halo clusters). At the distance of NGC 1311, this corresponds to $0''.12$, or about 1.2 WFC pixels. Figure 9 shows a histogram of the observed half-light radii of our candidate clusters, along with those of the comparison stars used in Fig. 8. There is a group of objects that are marginally resolved (comparable to globular clusters at the distance of NGC 1311), and another group that is much more extended. The most extended objects are also the fainter ones (candidates 8, 11 and 13). It may be that these objects are background galaxies, or statistical fluctuations in the disk of NGC 1311. However, they have physical sizes ($R_{hl} \approx 10$ pc) and absolute magnitudes ($M_V \approx -5$ to -7) similar to those of Galactic open clusters (see Table 6.2 of Binney & Merrifield 1998).

4.2. Background and Foreground Contamination

We note that all of the compact candidates were identified as such because their colors are unusual for luminous hot stars. Possible sources of contamination are foreground (Galactic) stars, background QSOs, and blending of stars in NGC 1311. The five compact sources are all within the $48'' \times 80''$ region shown in Fig. 4, and all have $V_{606} \lesssim 22.6$. The expected foreground Galactic stellar contamination down to this magnitude level is less than one star (Ratnatunga & Bahcall 1985). It seems unlikely from this that all five sources are foreground stars. We shall return to this point when we consider photometric modelling of the source colors below.

⁸We used the February 2003 database revision available at <http://www.physics.mcmaster.ca/Fac.Harris/Databases.html>.

It is unlikely the sample is contaminated by background QSOs. Based on the bright QSO number counts of Koo & Kron (1982), we expect an average of 0.07 QSOs with $V_{606} \lesssim 22.6$ in our $48'' \times 80''$ field of view.

4.3. Analysis of Cluster Photometry

4.3.1. Aperture Correction

As noted in §3.1 above, we used HSTPhot to perform aperture photometry on our WFPC2 data, and measured our own set of aperture corrections for the NICMOS photometry. In both cases we expect excellent photometric results (statistical errors of $\lesssim 0.05$ mag for sources brighter than 22nd mag) for stellar sources. But even marginally resolved sources, such as compact clusters, will require different aperture corrections than individual stars. While HSTPhot is able to deliver excellent photometry for marginally resolved clusters (Dolphin & Kennicutt 2002a; 2002b), some of our sources are clearly well-resolved. We thus adopted the more general methodology for aperture correction of HST/WFPC2 data from Anders et al. (2006).

We began by fitting circular 2-D Gaussians to each of the 13 candidate clusters in the F606W image. We then chose source and sky apertures and cluster light profiles for each object. Typically the source aperture was 1 to 2 pixels larger than the measured full width at half-maximum (FWHM) of the Gaussian fit, and the sky apertures were 2 (inner) and 4 (outer) pixels larger than the source aperture. Note that this will subtract counts due to both the sky and to diffuse light in NGC 1311 that is smooth on angular scales of $\lesssim 4$ WFC pixels ($0''.4$). This will also subtract the extended cluster light, however that flux should be accounted for the by aperture correction, as discussed below.

We used the formalism of Anders et al. (2006) to determine aperture corrections for each source. As Anders et al. (2006) model aperture corrections for the F555W, but not the F606W filter, we must assume that there is no significant aperture-correction color term between the F555W and F606W filters. As the characteristic wavelengths of the two filters differ by only $\approx 650\text{\AA}$, this is not unreasonable. For the compact, red objects (candidates 1, 7 and 10) we used the King30 profile (a King 1962 profile with $r_t/r_c = 30$, corresponding to a concentration index of 1.48). This profile is appropriate for star clusters that are old enough to be tidally truncated (King 1962). For the bluer objects (all the others) we used the EFF15 profile (an Elson et al. 1987 profile with a power-law index of 1.5), as star clusters in the nearby galaxies are better-fit with power-law profiles than with King models (e.g., Mackey & Gilmore 2003; de Grijs & Anders 2006 and references therein).

The measured FWHMs from the F300W and F814W frames are statistically consistent with those found from the F606W frame, but are less well determined due to the lower signal-to-noise ratio in these shallower images. Given this, we decided to apply the F606W aperture corrections to the much shallower F814W and F300W data. This is reasonable unless there is significant mass segregation in the target clusters. For young clusters, mass segregation can cause both the F300W and F814W profiles to be more concentrated than the F606W profile, due to the massive main-sequence stars and red supergiants, respectively. For old clusters, mass segregation can also cause both the F300W and F814W profiles to be more concentrated than the F606W profile, due to the hot horizontal branch stars and upper RGB and AGB stars respectively. In both cases, the F606W aperture correction will be an overcorrection for the other bands. It is impossible to predict how much of a problem this will be for a given cluster because of statistical sampling of the stellar mass function (e.g., Johnson et al. 2001). Except for very populous clusters, the number of stars in the various evolutionary states in question is very small. We discuss this possibility further in §4.3.2, below.

Our NICMOS data were obtained with the NIC3 camera. There are no Anders et al. (2006) aperture corrections for the NIC3 camera. However, the large pixel size and PSF of the NIC3 camera makes aperture correction a less severe problem than for our WFPC2 data. Our 2-pixel radius aperture has an angular radius of $\approx 0''.4$, or about 4 WFC pixels. This is larger than the F606W FWHM for most of the cluster candidates. The exceptions are candidates 2, 8, 11 and 13. Candidate 8 is undetected in the NICMOS image. For the other candidates, we measured the flux at radii larger than 2 NIC3 pixels. The inclusion of this flux would amount to an additional correction that is small compared to the standard aperture correction (0.1 mag). We thus make no further adjustments to the aperture corrections for our NIC3 data.

In Table 3 we present our photometric measurements for each of the candidate star clusters. Column 1 is a serial ID. Column 2 shows the unprocessed (X,Y) pixel locations on individual chips of the F606W frame in the upper row, and the J2000.0 Right Ascension and declination in the lower row. Column 3 shows which chip the cluster is located on in the F606W frame. The upper rows of columns 4–7 give the apparent magnitudes in F300W (UV_{300}), F606W (V_{606}), F814W (I_{814}) and F160W (H_{160}) for the cluster candidates, and columns 8–13 give the resulting colors. The errors on these quantities are given in the lower rows.

4.3.2. *Modelling of Cluster Photometry*

We have analysed the photometry for the candidate clusters that are detected in all four passbands with AnalySED (de Grijs et al. 2003a; Anders et al. 2004b). For our adopted distance and metallicities of $Z = 0.004$ and 0.008 , this results in a set of ages, extinctions, and masses for these candidate star clusters. As noted in §3.1, above, the $Z = 0.004$ are generally a better match to the single-star photometry, and metallicities larger than 0.008 are clearly inconsistent with the observed F300W magnitudes. We built models with both metallicities to bracket the plausible values for the star clusters. The results are given in Table 4. We generated fits using both the Cardelli et al. (1989) and the Calzetti (1997) extinction laws. The results for the two extinction laws are generally consistent with one another at the 1σ level. The values and errors quoted in Table 4 reflect the range of results for the two extinction laws.

The ages from AnalySED fall into three broad ranges. The youngest clusters have ages of $\lesssim 10$ Myr (#s 3 & 5). There is an intermediate age group with ages of ~ 100 Myr (#s 1, 4, 6 & 12). Finally, there are two clusters with ages $\gtrsim 1$ Gyr (#s 7 & 10). We note that the photometry for cluster 7 is consistent with a much younger age if $Z = 0.008$. However, such a young age also requires an extinction that is both much higher than the foreground extinction (Schlegel et al. 1998), and the typical internal extinction for low-luminosity late-type galaxies. Furthermore, the images of NGC 1311 (see Fig. 1) show no evidence for regions of strong localized extinction. For these reasons, we believe the age result for the $Z = 0.004$ is more plausible for cluster 7.

In Figure 10, we plot cluster age against cluster mass from the AnalySED results for $Z = 0.004$ (the plot for $Z = 0.008$ is similar). We include the candidates detected in only two passbands (see Table 3). There is a clear positive trend. Both the Spearman rank and the Kendall’s τ tests return probabilities of correlation of $>99\%$, despite the small sample. The line is a simple linear bisector, showing that the data are well-described by a power law. We hasten to point out that several effects can contribute to the appearance of such a plot, and that the resulting fit parameters are, therefore, unlikely to have a single physical interpretation: The scarcity of old, low-mass clusters may reflect the detection limit of the sample, but can also follow from the dynamics of cluster dissolution (e.g., Gieles et al. 2005). NGC 1311 shows no signs of the massive, young super star-clusters that form in strong starbursts (e.g., Whitmore et al. 1999). Its recent cluster formation history is similar to that of other undisturbed, low-luminosity, late-type galaxies (e.g., Billett et al. 2002; Mora et al. 2007).

We can also study the properties of the candidate clusters, including those that are only detected in a subset of our pass-bands, with less data-intensive techniques. In Figure 11 we present two color-color diagrams of the cluster candidates, along with predictions of the

Girardi et al. (2002) SSP models. The models shown in Fig. 11 all have Solar heavy-element abundance ratios, and include convective overshooting. Comparisons with α -enhanced models do not change the qualitative results shown in Fig. 11. Most of the candidate clusters are consistent with low-metallicity models with ages in the range 3–100 Myr. Two cluster candidates (#s 4 & 12) have colors that lie off all the SSP models. Consideration of all the color-color plots indicate that both these objects are either too red compared to SSP models (that is, they are too bright in both F814W and F160W), or too bright in F300W. This argues against a calibration systematic, as the problem appears in both the WFPC2 and NICMOS data. Both of these objects were initially flagged as candidate clusters based on their colors. One of the two objects (#12) is unresolved, and the other (#4) is marginally resolved. This suggests that, perhaps, these are cases of close blends of bright stars with significantly different colors. It is also possible that these objects are examples of clusters that have experienced significant mass-segregation. As noted in §4.3.1, above, we expect that the F606W aperture corrections would *overcorrect* the F300W magnitudes for mass-segregated clusters. This could lead to the blueward displacement that we find for these clusters in Fig. 11.

Two cluster candidates (#s 7 & 10) have implied ages of $\gtrsim 1$ Gyr from both the AnalySED fits and the Girardi et al. (2002) SSP models. The observed colors are consistent with Girardi et al. (2002) model ages as large as those of ancient Galactic globular clusters, although the AnalySED fits and the observed colors argue for ages younger than a few Gyr. Both objects are marginally resolved, and would have absolute magnitudes of $M_{606} \approx -7.9$ and -7.6 at the distance of NGC 1311. Accounting for the color term between F606W and the standard Johnson V -band, this is well within the range of globular cluster absolute magnitudes (Ashman & Zepf 1998). These are thus candidate intermediate-age globular star clusters. They could possibly be foreground stars, but the absolute magnitudes implied by their colors ($M_{606} \approx +6$ to $+7$) would place them at a distance of 5 to 6 kpc. This is highly unlikely for a line of sight with $b \approx -53^\circ$.

4.4. Cluster Formation History

Studies of the star formation history of low-luminosity galaxies generally conclude that star formation occurs in brief bursts separated by relatively long quiescent periods (e.g., Hunter 1997; Mateo 1998; Hunter & Elmegreen 2004; Corbin et al. 2007), during which star formation can still continue at a low level (van Zee 2001). In the most extreme cases, the light from young massive star clusters dominates the bolometric output of ultracompact blue dwarf galaxies (e.g., Corbin et al. 2005; Corbin et al. 2006), despite the presence of

much more massive old stellar populations. Typical late-type dwarf galaxies are also known to be rich in populous star clusters (Billett et al. 2002; Anders et al. 2004a). The Magellanic Clouds are our prototypes for star-forming low-luminosity galaxies. As such, much of our understanding of the importance of star clusters in such galaxies follows from studies of Magellanic Cloud clusters (e.g., de Grijs & Anders 2006 and references therein). Such studies can help us understand the factors governing the onset of bursts of star formation in systems that are generally not dominated by coherent large-scale phenomena like density waves. Both the results of the detailed four-band AnalySED method (de Grijs et al. 2003a; Anders et al. 2004b), and those of the simpler SSP color-color plots argue for three epochs of cluster formation in NGC 1311, with ages of ~ 10 Myr, ~ 100 Myr, and $\gtrsim 1$ Gyr. Our data for the individual stars (see Fig. 3) show the two younger episodes clearly, but cannot probe the oldest event, as $\gtrsim 1$ Gyr-old stars are too faint and red to be detected in our data.

5. Summary and Conclusions

NGC 1311 is a nearby, but little studied, low-luminosity late-type spiral. It has optical and H I properties (see Table 1) typical for such galaxies (Mateo 1998; van Zee 2001). It is a member of a loose association of galaxies (Tully et al. 2006), but displays no obvious sign of any recent interaction. We have used HST WFPC2 and NICMOS images of NGC 1311, that span the near-UV through the near-IR, to identify a small population of 13 candidate star clusters. Their masses increase systematically with cluster age, as would follow from the fading and dissolution of old, low-mass clusters, and the lack of any young super star clusters associated with strong starbursts. Half the cluster candidates are significantly fainter than the turnover of the globular cluster luminosity function. We are thus probing the range of luminosities typical of the faint star clusters found in Local Group dwarf galaxies, and the open cluster population of the Galactic disk. Analysis of the photometry of the candidate star clusters suggests that NGC 1311 has had three cluster-forming episodes in its history, occurring ~ 10 Myr, ~ 100 Myr, and $\gtrsim 1$ Gyr ago. This is consistent with observational work on other nearby low-luminosity galaxies indicating a bursting mode of star-formation. The recent star formation, as traced by the NUV continuum (see Fig. 1a), is concentrated at the east and west ends of the central bulge-like concentration. This is reminiscent of stochastic star formation models (Seiden et al. 1979) as well as the observed properties of other low-luminosity star-forming galaxies (e.g., Sextans A; Dohm-Palmer et al. 2002). NGC 1311 is an excellent example of a nearby, low-luminosity, star-forming, gas-rich galaxy that is evolving in relative isolation. Understanding the star- and cluster-formation history and chemical evolution of such galaxies is an essential part of unraveling the problem of galaxy evolution.

Our next step is a study of the resolved stellar populations of NGC 1311 with our combined WFPC2/NICMOS HST data. The large wavelength range of our data allows us to sample both the very recent star formation (dominating the UV light) and the ancient stellar populations (from the red/near-IR light) that appear ubiquitous even in very late-type galaxies (e.g., Baade 1958; Taylor et al. 2005). This should give us a clearer picture of the star formation history in this system, and a fuller understanding of the process of star formation in low-luminosity late-type galaxies in general.

PBE would like to thank the Department of Physics & Astronomy at Minnesota State University for support during this project. We thank Andy Dolphin for answering the first author’s HSTPhot questions with patience. We are grateful to our referee for a report that led up to significantly improve this paper. This research has made use of NASA’s Astrophysics Data System Bibliographic Services, and the NASA/IPAC Extragalactic Database (NED) which is operated by the Jet Propulsion Laboratory, California Institute of Technology, under contract with the National Aeronautics and Space Administration. PA acknowledges support by the DFG grant Fr 911/11-3. This work was supported in part by NASA Hubble Space Telescope grants HST-GO-09124* and HST-GO-09824* awarded by the Space Telescope Science Institute, which is operated by AURA for NASA under contract NAS 5-26555.

Facilities: HST

REFERENCES

- Anders, P., Bissantz, N., Boysen, L., de Grijs, R., & Fritze-v. Alvensleben, U., 2007, MNRAS, 377, 91
- Anders P., Bissantz N., Fritze-von Alvensleben U., & de Grijs R., 2004b, MNRAS, 347, 196
- Anders, P., de Grijs, R., Fritze-v. Alvensleben, U., & Bissantz, N., 2004a, MNRAS, 347, 17
- Anders, P., Gieles, M., & de Grijs, R., 2006, A&A, 451, 375
- Ashman, K. M. & Zepf, S. E. 1998, *Globular Cluster Systems* (Cambridge, Cambridge Univ. Press).
- Baade, W. 1958, in *Ricerche Astronomiche*, v. 5, Proceedings of a Conference at Vatican Observatory, ed. D.J.K. O’Connell (Amsterdam: Interscience), 303
- Bastian, N., Gieles, M., Lamers, H. J. G. L. M., Scheepmaker, R. A., & de Grijs, R. 2005, A&A, 431, 905

- Billett, O. H., Hunter, D. A., & Elmegreen, B. G., 2002, *AJ*, 123, 1454
- Binney, J., & Merrifield, M., 1998, *Galactic Astronomy* (Princeton Univ. Press: Princeton)
- Calzetti, D., 1997, *AJ*, 113, 162
- Cardelli, J. A., Clayton, G. C., & Mathis, J. S. 1989, *ApJ*, 345, 245
- Corbin, M. R., Kim, H., Jansen, R. A., Windhorst, R. A. & Cid Fernandes, R. 2007, *ApJ*,
In press
- Corbin, M. R., Vacca, W. D., Cid Fernandes, R., Hibbard, J. E., Somerville, R. S., &
Windhorst, R. A. 2006, *ApJ*, 651, 861
- Corbin, M. R., Vacca, W. D., Hibbard, J. E., Somerville, R. S., & Windhorst, R. A. 2005,
ApJ, 629, L89
- de Grijs, R., Anders, P., Lamers, H. J. G. L. M., Bastian, N., Fritze-v. Alvensleben, U.,
Parmentier, G., Sharina, M. E., & Yi, S. 2005, *MNRAS*, 359, 874
- de Grijs R. & Anders, P. 2006, *MNRAS*, 366, 295.
- de Grijs R., Fritze-von Alvensleben U., Anders P., Gallagher J. S. III, Bastian N., Taylor
V. A., & Windhorst R. A., 2003, *MNRAS*, 342, 259
- de Grijs, R., Lee, J. T., Mora Herrera, M. C., Fritze-v. Alvensleben, U., & Anders, P., 2003,
New A, 8, 155
- de Jong, R. S. 2006, “Correcting NICMOS Count-Rate Dependent Non-linearity,” NICMOS
Instrument Science Report 2006-003 (Baltimore: STScI).
- de Vaucouleurs, G., de Vaucouleurs A., Corwin, H. G., Jr., Buta, R. J., Paturel, G. & Fouqué,
P. 1991, *Third Reference Catalogue of Bright Galaxies* (Springer-Verlag: New York)
(RC3)
- Dohm-Palmer, R. C., Skillman, E. D., Mateo, M., Saha, A., Dolphin, A., Tolstoy, E., Gal-
lagher, J. S., & Cole, A. A. 2002, *AJ*, 123, 813
- Dolphin, A. E. 2000, *PASP*, 112, 1383
- Dolphin, A. E. & Kennicutt, R. C., Jr. 2002, *AJ*, 123, 207
- Dolphin, A. E. & Kennicutt, R. C., Jr. 2002, *AJ*, 124, 158
- Elson, R. A. W., Fall, S. M., & Freeman, K. C. 1987, *ApJ*, 323, 54

- Gallart, C., Zoccali, M., Bertelli, G., Chiosi, C., Demarque, P., Girardi, L., Nasi, E., Woo, J.-H., Yi, S. 2003, *AJ*, 125, 742
- Gieles, M., Bastian, N., Lamers, H. J. G. L. M., & Mout, J. N. 2005, *A&A*, 441, 949
- Girardi, L., Bertelli, G., Bressan, A., Chiosi, C., Groenewegen, M. A. T., Marigo, P., Salasnich, B., & Weiss, A. 2002, *A&A*, 391, 195
- Harris, W. E. 1996, *AJ*, 112, 1487
- Hodge, P. W. 1961, *ApJ*, 133, 413
- Holtzman, J. A., Burrows, C. J., Casertano, S., Hester, J. J., Trauger, J.T., Watson, A. M., & Worthey, G. 1995, *PASP*, 107, 1065
- Hunter, D. A. 1997, *PASP*, 109, 937
- Hunter, D. A., & Elmegreen, B. G. 2004, *AJ*, 128, 2170
- Johnson, R. A., Beaulieu, S. F., Gilmore, G. F., Hurley, J., Santiago, B. X., Tanvir, N. R., Elson, R. A. W. 2001, *MNRAS*, 324, 367
- King, I. 1962, *AJ*, 67, 471
- Koo, D. C. & Kron, R. G., 1982, *A&A*, 105, 107
- Koribalski, B. S., Staveley-Smith, L., Kilborn, V. A., Ryder, S. D., Kraan-Korteweg, R. C., Ryan-Weber, E. V., Ekers, R. D., Jerjen, H., Henning, P. A., Putman, M. E., Zwaan, M. A., de Blok, W. J. G., Calabretta, M. R., Disney, M. J., Minchin, R. F., Bhathal, R., Boyce, P. J., Drinkwater, M. J., Freeman, K. C., Gibson, B. K., Green, A. J., Haynes, R. F., Juraszek, S., Kesteven, M. J., Knezek, P. M., Mader, S., Marquarding, M., Meyer, M., Mould, J. R., Oosterloo, T., O'Brien, J., Price, R. M., Sadler, E. M., Schröder, A., Stewart, I. M., Stootman, F., Waugh, M., Warren, B. E., Webster, R. L., & Wright, A. E. 2004, *AJ*, 128, 16
- Larsen, S. S. 2004, *A&A*, 416, 537
- Mackey, A. D. & Gilmore, G. F., 2003, *MNRAS*, 338, 85
- Maraston, C. 2005, *MNRAS*, 362, 799
- Mateo, M. L. 1998, *ARA&A*, 36, 435
- Mora, M. D., Larsen, S. S., & Kissler-Patig, M. 2007, *A&A*, 464, 495

- Noll, K. et al. 2004 "NICMOS Instrument Handbook", Version 7.0, (Baltimore: STScI).
- Persson, S. E., Aaronson, M., Cohen, J. G., Frogel, J. A. & Matthews, K. 1983, ApJ, 266, 105
- Ratnatunga, K. U. & Bahcall, J. N., 1985, ApJS, 59, 63
- Schlegel, D. J., Finkbeiner, D. P. & Davis, M. 1998, ApJ, 500, 525
- Seiden, P. E., Schulman, L. S., & Gerola, H. 1979, ApJ, 232, 702
- Seth, A., Olsen, K., Miller, B., Lotz, J. & Telford, R. 2004, AJ, 127, 798.
- Stetson, P. B. 1987, PASP, 99, 191
- Stover, R. J., 1988, in "Instrumentation for Ground-based Optical Astronomy: Present and Future," ed. L.B. Robinson (Springer: New York), p. 443
- Taylor, V. A., Jansen, R. A., Windhorst, R. A., Odewahn, S. C. & Hibbard, J. E. 2005, ApJ, 630, 784
- Tully, R. B., Rizzi, L., Dolphin, A. E., Karachentsev, I. D., Karachentseva, V. E., Makarov, D. I., Makarova, L., Sakai, S., & Shaya, E. J., 2006 AJ, 132, 729
- van Zee, L. 2001, AJ, 121, 2003
- Whitmore, B. C., Qing, Z., Leitherer, C., Fall, S. M., Schweizer, F. & Miller, B. W. 1999, AJ, 118, 1551.
- Windhorst, R. A., Taylor, V. A., Jansen, R. A., Odewahn S. C., Chiarenza, C. A. T., de Grijs, R., de Jong, R. S., Frogel, J. A., Eskridge, P. B., Gallagher, J. S., Conselice, C., Hibbard, J. E., Matthews, L. D., MacKenty, J. & O'Connell, R. W. 2002, ApJS, 143, 113

Fig. 1.— $42'' \times 26''$ images of NGC 1311 in a) F300W, b) F606W, c) F814W, and d) F160W. The arrow in the upper-left corner of the F300W image points North, the attached line-segment points East. The scale bar in the lower-right corner of the F300W image is $10''$, and applies to all four panels.

Fig. 2.— Stellar color-color diagrams in a) $(UV_{300} - I_{814})$ vs. $(V_{606} - I_{814})$, and b) $(UV_{300} - V_{606})$ vs. $(UV_{300} - I_{814})$. Solid circles with error-bars show the data. The arrows in each plot show the foreground dereddening vectors. The isochrones (Girardi et al. 2002) have $Z=0.004$, and cover a range in age from 4 Myr to 6 Gyr.

Fig. 3.— F606W vs. $(F606W - F814W)$ Color-Magnitude diagram with symbols and isochrones as in Fig. 2. The solid lines are the 10 Myr and 100 Myr isochrones. The dotted lines are younger, intervening, and older isochrones, sampled every 0.25 dex in age. The points surrounded by large circles indicate objects with peculiar colors, as discussed in the text. The dashed line shows $I_{814} = 22$. The points surrounded by large diamonds are objects with peculiar colors, but fainter than this limit. The bold arrow shows the foreground dereddening vector.

Fig. 4.— A $48'' \times 80''$ region of the F606W image in which the photometrically selected candidate clusters are circled.

Fig. 5.— Sharpness vs. V_{606} . Circled points are the photometrically selected candidate clusters. Plus-signs are single-pixel objects that HSTPhot classifies as either hot pixels or cosmic rays. Points enclosed in diamonds are classified as “extended sources” by HSTPhot. The diamonds with large, dark crosses overlaid appear to be background galaxies based on Figure 6.

Fig. 6.— The full WFPC2 F606W image, showing the photometrically selected candidate clusters as in Fig. 4, and additional faint cluster candidates enclosed in diamonds. Note that two of the four background objects are obvious background spirals.

Fig. 7.— $6''.5$ square “postage stamps” of the candidate clusters shown in Fig. 6, not including the clear background spirals.

Fig. 8.— Radial profiles of cluster candidates along with stars from the corresponding WF chips. The stellar profiles are the solid, bold lines. a) WF2 clusters 1–2, b) WF3 clusters 3–6, c) WF3 cluster 7–11 d) WF4 clusters 12–13.

Fig. 9.— Histogram of observed half-light radii of candidate clusters (solid line) along with those of the comparison stars (dotted line).

Table 1. Basic Properties

		References
m_B	13.22 ± 0.21	1
$(B - V)$	0.46 ± 0.02	1
V_\odot	568 ± 5 km/sec	2
A_V	0.07	3
$E(B - V)$	0.021	3
D	5.45 ± 0.08 Mpc	4
M_B	-15.5	1,4
S_{HI}	15.4 Jy km/sec	2
M_{HI}/L_B	$0.46 M_\odot/L_\odot$	1,2,4

References. — 1) de Vaucouleurs et al. (1991); 2) Koribalski et al. (2004); 3) Schlegel et al. (1998); 4) Tully et al. (2006)

Table 2. Log of Observations

Data Set	PID	Camera/Filter	Date	Exposure
			dd-mm-yyyy	sec
u6dw7101m	9124	WFPC2/F300W	27-08-2001	300
u6dw7102m	9124	WFPC2/F300W	27-08-2001	300
u6g22403m	9162	WFPC2/F606W	22-09-2001	300
u6g22404m	9162	WFPC2/F606W	22-09-2001	300
u6dw7103m	9124	WFPC2/F814W	27-08-2001	40
u6dw7104m	9124	WFPC2/F814W	27-08-2001	40
n8ou36010	9824	NIC3/F160W	28-11-2003	512

Table 3. Photometry of Cluster Candidates

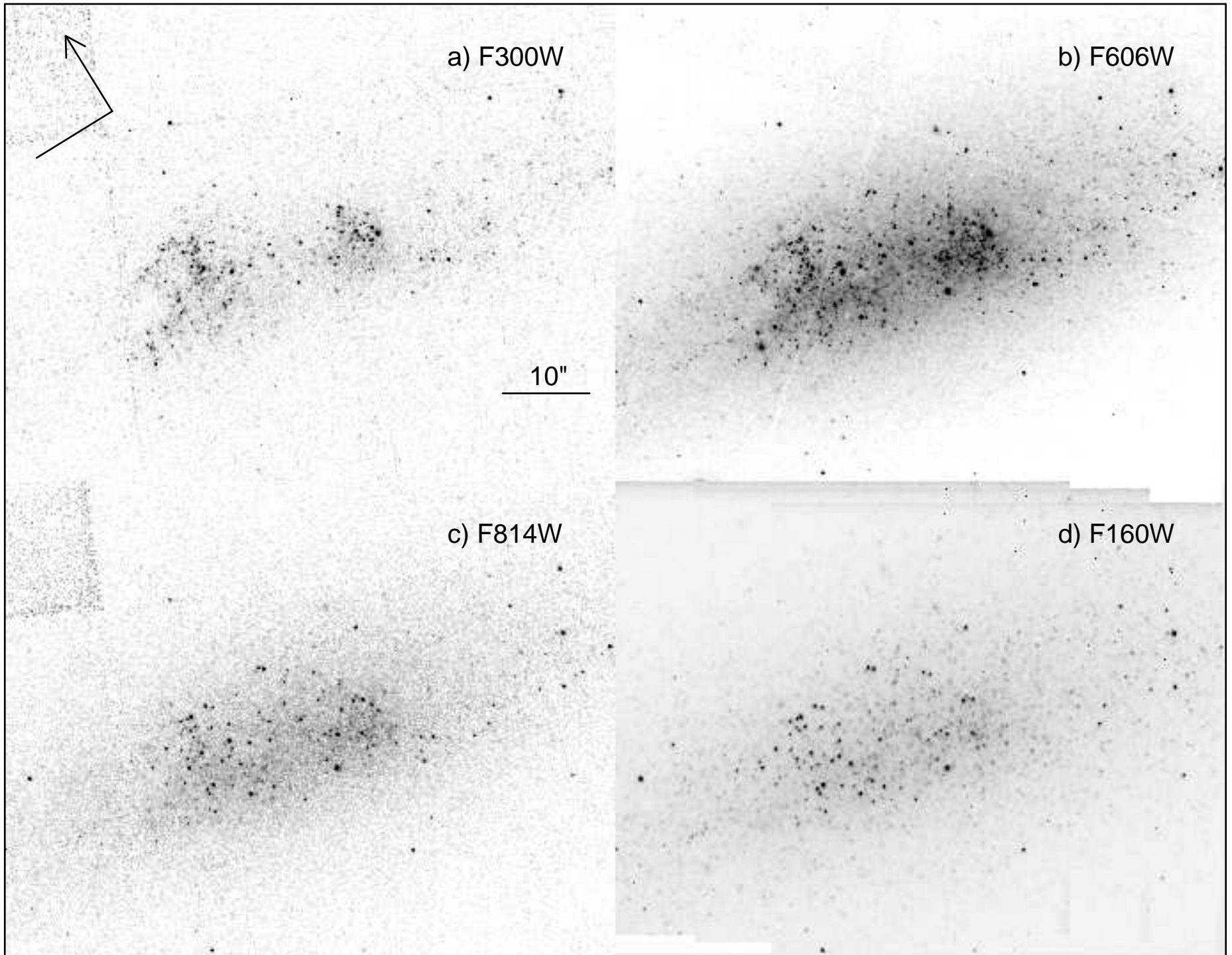
ID	(X_{606}, Y_{606})	chip	UV_{300}	V_{606}	I_{814}	H_{160}	(UV–V)	(UV–I)	(UV–H)	(V–I)	(V–H)	(I–H)
	RA, Dec (J2000.0)		e_{UV}	e_V	e_I	e_H	e_{UV-V}	e_{UV-I}	e_{UV-H}	e_{V-I}	e_{V-H}	e_{I-H}
1	188.20,336.93	WF2	20.44	20.27	20.02	18.89	0.18	0.43	1.55	0.25	1.38	1.13
	03:20:09.0,–52:10:39		0.09	0.01	0.03	0.02	0.09	0.10	0.09	0.04	0.02	0.04
2	57.97, 96.31	WF2		20.97		16.75					4.22	
	03:20:06.8,–52:10:56			0.01		0.07					0.07	
3	195.21,130.89	WF3	18.88	20.25	20.65	20.52	–1.38	–1.78	–1.64	–0.40	–0.27	0.13
	03:20:08.0,–52:11:04		0.04	0.02	0.11	0.06	0.05	0.11	0.08	0.11	0.07	0.12
4	203.02,170.29	WF3	21.51	22.12	21.42	19.63	–0.61	0.09	1.88	0.70	2.49	1.79
	03:20:08.2,–52:11:07		0.12	0.02	0.12	0.03	0.12	0.17	0.13	0.12	0.04	0.13
5	154.26,143.11	WF3	20.38	20.78	20.72	20.03	–0.40	–0.33	0.35	0.07	0.75	0.69
	03:20:07.6,–52:11:06		0.05	0.01	0.06	0.04	0.05	0.08	0.07	0.06	0.05	0.07
6	125.77,141.02	WF3	21.74	21.50	21.26	20.15	0.24	0.49	1.59	0.24	1.35	1.11
	03:20:07.3,–52:11:06		0.12	0.01	0.08	0.05	0.12	0.14	0.13	0.08	0.05	0.09
7	171.41,208.14	WF3	21.24	20.12	19.42	18.30	1.11	1.81	2.94	0.70	1.82	1.12
	03:20:07.9,–52:11:12		0.11	0.01	0.04	0.02	0.11	0.12	0.11	0.04	0.02	0.04
8	90.50,236.72	WF3	20.53	21.42			–0.89					
	03:20:07.2,–52:11:17		0.21	0.01			0.21					
9	113.51,265.14	WF3		21.55		19.97					1.58	
	03:20:07.4,–52:11:19			0.01		0.29					0.29	
10	87.64,268.90	WF3	21.94	20.69	20.14	18.79	1.25	1.81	3.15	0.55	1.90	1.35
	03:20:07.2,–52:11:19		0.16	0.02	0.08	0.02	0.16	0.18	0.16	0.08	0.03	0.08
11	76.61,273.71	WF3		23.05		19.43					3.62	
	03:20:07.1,–52:11:20			0.01		0.03					0.03	
12	209.90, 59.05	WF4	21.17	22.02	21.08	19.34	–0.84	0.10	1.83	0.94	2.68	1.74
	03:20:06.3,–52:11:15		0.10	0.03	0.10	0.03	0.10	0.14	0.10	0.10	0.04	0.10
13	200.42,111.80	WF4		21.93		19.89					2.04	
	03:20:05.7,–52:11:16			0.01		0.25					0.25	

Table 4. Candidate Cluster Properties from AnalySED

ID	Z	Age	$E(B - V)$	Mass
		Myr		$10^3 M_{\odot}$
1	0.004	92^{+10}_{-84}	$0.13^{+0.25}_{-0.05}$	$40.9^{+3.2}_{-29.5}$
	0.008	104^{+6}_{-67}	$0.05^{+0.18}_{-0}$	$35.9^{+9.6}_{-15.9}$
3	0.004	4 ± 0	0.00 ± 0	2.38 ± 0
	0.008	4 ± 0	0.05 ± 0	3.52 ± 0.06
4	0.004	128 ± 4	0.00 ± 0	$8.18^{+0.14}_{-0.05}$
	0.008	130^{+70}_{-6}	0.15 ± 0.03	$7.42^{+1.88}_{-0.14}$
5	0.004	8 ± 0	0.15 ± 0	3.82 ± 0.20
	0.008	4^{+2}_{-0}	$0.38^{+0.03}_{-0}$	$6.29^{+5.44}_{-0}$
6	0.004	54 ± 46	$0.25^{+0.13}_{-0.15}$	$8.24^{+5.81}_{-4.65}$
	0.008	100^{+10}_{-61}	$0.10^{+0.18}_{-0.05}$	$13.2^{+5.45}_{-6.90}$
7	0.004	844^{+124}_{-90}	0.00 ± 0	129^{+12}_{-9}
	0.008	4^{+846}_{-0}	$0.88^{+0.07}_{-0.88}$	$50.4^{+23.3}_{-4.6}$
10	0.004	976^{+150}_{-610}	$0.00^{+0.40}_{-0}$	$79.7^{+2.7}_{-34.1}$
	0.008	209^{+1800}_{-35}	$0.64^{+0.01}_{-0.64}$	$47.8^{+82.7}_{-14.1}$
12	0.004	128^{+0}_{-4}	0.00 ± 0	$10.5^{+0}_{-0.1}$
	0.008	12^{+74}_{-0}	$0.33^{+0.02}_{-0.33}$	$6.43^{+4.59}_{-0.26}$

Fig. 10.— Age vs. mass from AnalySED with $Z = 0.004$ for the candidate clusters. The line is a simple linear bisector.

Fig. 11.— Color-color diagrams of the candidate clusters (large black squares), along with the Girardi et al. (2002) SSP models for a range of metallicities (color-coded in the figure) and ages (symbols coded in the figure) a) $(UV_{300} - V_{606})$ vs. $(I_{814} - H_{160})$, b) $(UV_{300} - V_{606})$ vs. $(UV_{300} - H_{160})$.



a) F300W

b) F606W

c) F814W

d) F160W

10''

